

MARTIAN ULTRAVIOLET AURORA: RESULTS OF MODEL SIMULATIONS

J.-C. Gérard, LPAP, Université de Liège, Belgium (jc.gerard@ulg.ac.be), L. Soret, LPAP, Université de Liège, V.I. Shematovich, D.V. Bisikalo, INASAN, Russian Academy of Sciences, Moscow

Introduction:

Two types of aurorae excited by energetic electrons have been observed on the Mars nightside in the ultraviolet. The first one (discrete aurora) is very localized and appears to be controlled by the structure of the residual magnetic field in the southern hemisphere (Bertaux et al., 2005; Leblanc et al., 2008). Its characteristics have been determined by analyzing ten years of observations performed with Spectroscopy for the Investigation of the Characteristics of the Atmosphere of Mars (SPICAM) instrument on board Mars Express. The database has been searched to find signatures of ultraviolet emission different from the nitric oxide delta and gamma emissions frequently observed in the nightglow Martian spectrum. The most prominent signatures are the CO Cameron and CO₂⁺ doublet ultraviolet bands (UVD). A total of 113 nightside orbits with SPICAM pointing to the nadir in the region of residual magnetic field have been selected. Among them, 16 detections were unambiguously identified, some of them with multiple detections along an orbital track. Nightside limb observations were also analyzed leading to three positive detections.

A second type of Martian auroral emission (diffuse aurora), extending over a large fraction of the planet has been observed on several occasions with the Imaging Ultraviolet Spectrograph covering the spectral region extending from 110 to 340 nm (IUVS). The peak emissions are located near 65 km, an altitude significantly lower than the discrete aurora. The presence of this diffuse aurora was concurrent with enhanced solar activity in the extreme ultraviolet and the presence of energetic electrons up to 200 keV precipitating in the Martian upper atmosphere. The CO Cameron bands, CO₂⁺ ultraviolet doublet and OI 297.2 nm emissions are the prominent spectral features.

Morphology and characteristics of the discrete aurora:

These discrete auroral emissions are located in the vicinity of the statistical boundary between open and closed magnetic field lines (Figure 1). The mean energy of the electron energy spectra measured during concurrent ASPERA-3/ELS observations ranges from 150 to 280 eV. The ultraviolet aurora may be latitudinally displaced poleward or equatorward of the region of maximum enhanced downward electron energy flux by several tens of seconds and shows no direct proportionality with the electron flux measured at the spacecraft altitude. The small number of UV auroral detection in regions located along

crustal magnetic field structures where occasional aurora has been observed indicates that the Mars aurora is a rare transient feature. These results are consistent with the scenario of acceleration of electrons by transient parallel electric field along semi open magnetic field lines.

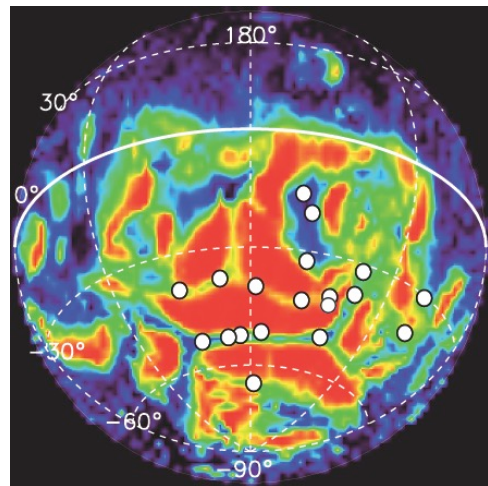


Figure 1: the circles indicate the locations of the aurora detected by SPICAM. The background colors show the increasing probability (from dark blue to red) that the magnetic field lines are closed. This map was derived from measurements on board MGS at about 400 km. This topology is in agreement with the assumption that electrons are precipitated in regions presenting a magnetic cusp structure. (ESA – Univ. de Liège).

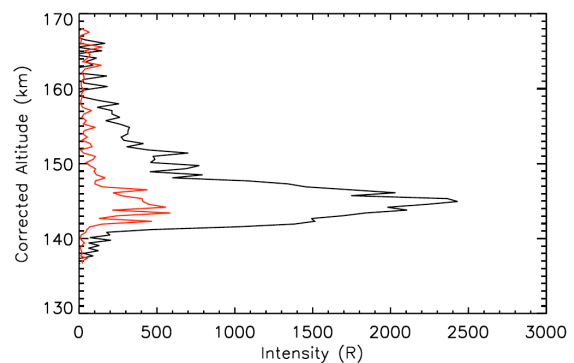


Figure 2: example of a limb emission profile of the UV discrete aurora measured with SPICAM. The apparent distribution (CO Cameron in black, CO₂⁺ UVD in red) has been corrected to account for the inhomogeneity of the emission region based on time delay between the four SPICAM spatial bins. The peak altitudes are located between 125 and 163 km, in agreement with the results of the electron transport model.

Characteristics of the diffuse aurora:

By contrast, the diffuse aurora was observed in the northern hemisphere, in the quasi absence of residual magnetic field. Since the aurora appeared fairly homogeneous during these periods, the altitude of the peak is assumed to coincide with the height of maximum signal. Emissions from the Cameron and CO_2^+ UVD bands and OI 297.2 nm were detected. Schneider et al. (2015) modeled the precipitated electron flux measured on 20 December 2014 with the SEP and SWEA detectors on board MAVEN between a few and 200 keV. They analytically fitted the combined electron energy spectrum (in particle flux units) with a $E^{-2.2}$ energy dependence. They obtained a good agreement with the shape and peak altitude of the observed CO_2^+ UV doublet limb profile. The peak intensity was normalized to the observed value. Further detections of diffuse aurora were made, related to other solar events.

Numerical modeling of auroral emission:

Monte Carlo model

The model is based on photochemical processes, kinetics and a Monte Carlo approach for vertical electron transport. Energetic electrons lose their kinetic energy in elastic, inelastic and ionizing collisions with the ambient atmospheric gas. The energy loss is calculated by solving the kinetic Boltzmann equation, involving transport of electrons, production rates of primary and secondary electrons and elastic and inelastic scattering terms. The Monte Carlo algorithm solves kinetic equations for atmospheric systems in the stochastic approach. It calculates the system evolution from the initial to the steady state between altitudes of 250 km and 50 km. The neutral atmosphere composition and density is based on the Mars Global Ionosphere-Thermosphere Model (M-GITM) (Bougher et al., 2015). The outputs of the model are calculated vertical emission profiles for various CO, CO_2^+ , O and C emissions. Further details about the Monte-Carlo model and its implementation for the Mars atmosphere were given by Schematovich et al. (2008).

Discrete aurora modeling

Nadir observations of aurorae have recently been analyzed in detail by Gérard et al. (2015). They quantified the intensities of the CO Cameron bands and the CO_2^+ doublet emissions, compared auroral events to concurrent electron precipitations and confirmed that aurorae occur near open-closed field line boundaries, in the Southern hemisphere between 150 and 225° of longitude.

Limb observations by Soret et al. (2015) detected the CO ($a^3\Pi - X^1\Sigma$) Cameron bands between 190 and 270 nm, the CO ($A^1\Pi - X^1\Sigma^+$) Fourth Positive sys-

tem (CO 4P) between 135 and 170 nm, the CO_2^+ ($B^2\Sigma_u^+ - X^2\Pi_g$) UV doublet at 289 nm, the OI at 297.2 nm and the 130.4 nm OI triplet emissions have been identified in the spectra and in the time variations of the signals. The intensities of these auroral emissions have been quantified and the altitude of the strongest emission of the CO Cameron bands has been estimated to be 137 ± 27 km. The observed altitudes of the auroral emissions were reproduced by the Monte-Carlo model of electron transport in the Martian thermosphere for monoenergetic electrons between 60 and 200 eV. No simple correlation was found between electron fluxes measured at the Mars Express altitude and nadir auroral intensity. Predicted vertically integrated intensities for the various auroral emissions were generally overestimated by the model. This is a possible consequence of the inclination and curvature of the magnetic field line threading the aurora. The relative brightness of the CO and CO_2^+ emissions was in good agreement with the observations.

The presence of a magnetic field modifies the electron energy spectrum and the ratio of the upward to the downward flux as the beam penetrates into a stronger region of stronger B-field (Bisikalo et al., 2016). Simulations based on an ASPERA-3 measured auroral electron precipitation indicate that magnetic mirroring leads to an change of the fraction of the energy flux carried by upward moving electrons (Figure 3). This fraction increases up to 33-78% in the presence of a field. Consequently, the presence of a remanent magnetic field results in a reduction of the total auroral power for given precipitated energy flux.

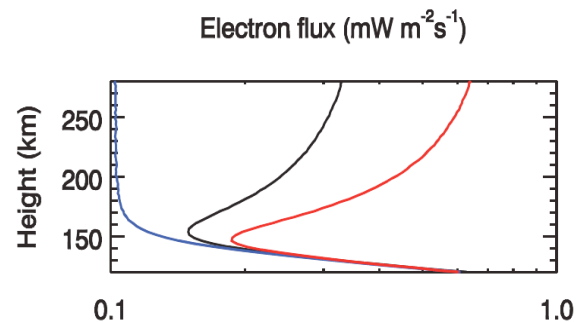


Figure 3: altitude variation of the ratio of upward to downward energy fluxes for three different crustal B-field intensities at 100 km: 0 (blue line), 23 (black line) and 150 nT (red line).

Diffuse aurora modeling

Monte Carlo simulations of the production of several ultraviolet and visible auroral emissions have been performed for monoenergetic initial electron energies between 0.1 and 200 keV. These emissions are the CO_2^+ UVD at 288.3 and 289.6 nm and the Fox-Duffendack-Barker (FDB) bands, the CO Cameron and CO 4P bands, the OI 130.4 and 297.2 nm multiplets and CI 156.1 nm and 165.7 nm features. We

present calculations of the nadir and limb intensities of several of these emissions for a unit precipitated energy flux of 1 mW/m^2 . Our results indicate that electrons in the range 100-200 keV produce maximum CO_2^+ UVD emission below 75 km. A peak near 65 km is obtained for electron energies of about 200 keV (Figure 4).

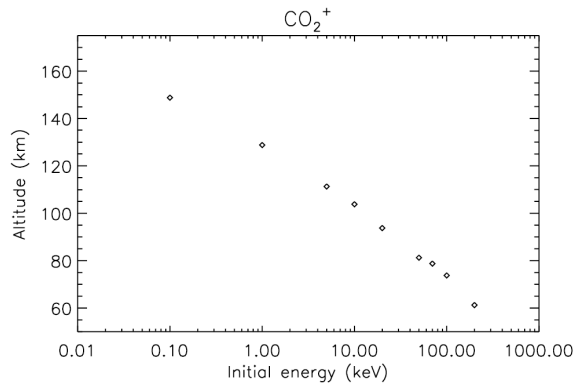


Figure 4: calculated peak altitude of the CO_2^+ UVD emission for a range of initial monoenergetic electron energies.

As mentioned before, SWEA and SEP electron energy spectra measured during diffuse aurora may be combined to calculate the volume emission rates. The strongest predicted emissions are the CO_2^+ FDB, UVD and the CO Cameron bands. The metastable a $^3\Pi$ state which radiates the Cameron bands is deactivated by collisions with CO_2 and CO below about 110 km. As a consequence, the ratio of the Cameron to the CO_2^+ UVD bands is predicted to decrease at low altitude in the energetic diffuse aurora (Figure 5).

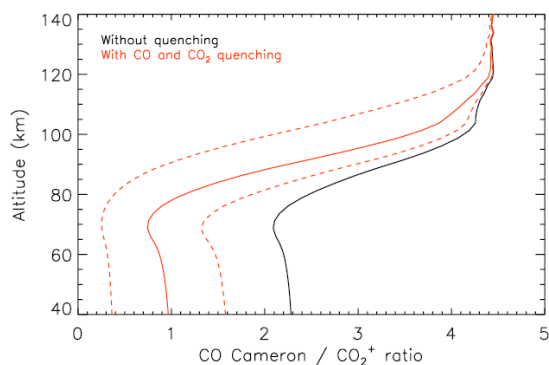


Figure 5: effect of collisional quenching on the limb intensity ratio of the Cameron/ CO_2^+ UVD bands. The initial electron energy in this case is 100 keV. Red solid line refers to standard values of the quenching coefficients and dotted lines indicate the extreme values.

Calculated limb profiles will be compared with the IUVS observations of the emission limb profiles reported by Schneider et al. (2015).

Conclusions:

Two clearly types of auroral events have been detected on the Mars nightside. Discrete aurorae appear as rare, localized events confined to regions in the southern hemisphere where the residual magnetic field cusp like structures. By contrast, the diffuse aurora has been observed in the field-free northern hemisphere, but it is strongly controlled by solar activity. The altitudes of the emissions are different in the diffuse aurora showing a peak located about 70 km lower than the discrete ones. The ultraviolet auroral spectrum appears quite similar in the two types of events. However, the upper state of the CO Cameron bands is deactivated by collisions at low altitudes and therefore decreases with respect to allowed emissions. Model calculations show indicate that the CO_2^+ Fox–Duffendack–Barker (FDB) bands which extend into the visible are among the strongest auroral emissions.

References:

- Bertaux, J.-L. et al. (2005), Discovery of an aurora on Mars. *Nature* 435, 790–794.
- Bisikalo, D.V. et al. (2016), Influence of the crustal magnetic field on the Mars aurora electron flux and UV brightness, *Icarus*, in press.
- Bougher, S. W. et al. (2015), Mars Global Ionosphere-Thermosphere Model: Solar cycle, seasonal and diurnal variations of the Mars upper atmosphere. *J. Geophys. Res.* 120, 311–342.
- Gérard, J. C., et al. (2015). Concurrent observations of ultraviolet aurora and energetic electron precipitation with Mars Express. *J. Geophys. Res.*, 120, 6749-6765.
- Leblanc, F. et al. (2008), Observations of aurorae by SPICAM ultraviolet spectrograph on board Mars Express: Simultaneous ASPERA-3 and MARSIS measurements. *J. Geophys. Res.* 113, A08311.
- Schneider, N. M. et al. (2015), Discovery of diffuse aurora on Mars, *Science*, 350, doi: 10.1126/science.aad0313.
- Shematovich, V.I. et al. (2008), Monte Carlo model of electron transport for the calculation of Mars dayglow emissions, *J. Geophys. Res.*, 113, E02011.
- Soret, L. et al. (2016), SPICAM observations and modeling of Mars aurorae, *Icarus*, 264, 398-406.